Gas Absorption into A Wavy Two-Layer Falling Film

G. Çekiç and G. M. Sisoev
School of Mathematics, University of Birmingham, Birmingham B15 2TT, United Kingdom

DOI 10.1002/aic.14778
Published online March 11, 2015 in Wiley Online Library (wileyonlinelibrary.com)

Absorption of a weakly soluble gas into a two-layer film flowing down a vertical wall is studied in the framework of an approximate long-wave model. It is shown that wavy regimes in the film strongly affect the absorption rate. © 2015 American Institute of Chemical Engineers *AIChE J*, 61: 2058–2069, 2015
Keywords: thin liquid film, interface, nonlinear waves, bifurcations, absorption

Introduction

There are many papers studying gas absorption in single-layer falling films but, to the best of our knowledge, the mass transfer in wavy two-layer films has not been modeled so far. The main difficulty in computing mass transfer in the two-layer film, as well as in the case of a single-layer film, is due to the complexity of solving the hydrodynamical problem to find finite-amplitude wave regimes. In this article, we find nonlinear wavy regimes and then generalize the approach developed in[1,2] to solve the diffusion problem for a weakly soluble gas.

Reviews of previous studies of gas absorption in single-layer films can be found in Refs. 1–7. Here, we briefly recap the principal results in the hydrodynamical theory of film flows and the modeling of mass transfer within them.

Systematic studies of film flows were initiated by the experimental work[8] where typical wave regimes were first identified. Most theoretical results have been reached using the Kapitza–Shkadov model[9] generalizing the Prandtl-Pohlhausen boundary layer method. Numerical methods have also been used to model film flows, see Refs. 10–12. Reviews of the film theory can be found in monographs[13,14] and latter works.[15–17]

Although researches have mainly been concentrated on single-layer films, a few studies dealing with two-layer films have also been published. The asymptotic method developed in[18] for a single-layer film was used in Refs. 19–21 to find two linear unstable modes associated with the film surface and the interface between two liquids. These modes were studied later in Refs. 22–25, where the generalized Orr–Sommerfeld problem was solved numerically.

A new model generalizing the Kapitza–Shkadov approach for the case of two-layer film flow has been developed in recent works.[26,27] Evolution scenarios of space-periodic waves were investigated in Ref. 26 by systematic transient computations, and principal families of steady-traveling space-periodic waves were computed in Ref. 27.

It is known from experiments that mass transfer in wavy single-layer liquid films is greater than those provided by the waveless flow,[28–34] and this amplification was observed at values of the Reynolds number when regular waves exist.

To model the absorption in wavy films, experimentally measured waves were used in[35] where the mass-transfer amplification was computed. The mass transfer in the case of theoretically computed waves in the falling film was studied in Ref. 1 where the amplification factors were computed at values of similarity parameters corresponding to real-life flow conditions.

In this article, we study the gas absorption into a wavy two-layer falling film. We begin from the hydrodynamical problem and find its solutions in the form of steady-traveling periodic waves in Section Film Hydrodynamics. In Section Mass Transfer, the governing equations of the gas absorption are analyzed and the numerical results are discussed in Section Results. Finally, conclusions are provided in Section Conclusions.

Film Hydrodynamics

Evolution equations

In this article, we consider a two-layer film flowing down a vertical wall. Liquids in the layers are assumed viscous, incompressible and immiscible.

To describe the flow, we use the Cartesian coordinate system (x, y) where the x-axis is oriented along the wall and points down, and the y-axis points into the film bulk. Parameters of the flow in the layers are referred to using upper indices 1 for the layer adjacent to the wall and 2 for the layer with the free surface. Then, the physical properties of the liquids are denoted as $\rho^{(1)}$ and $\rho^{(2)}$ for the densities, $\nu^{(1)}$ and $\nu^{(2)}$ for the kinematic viscosities in the first and second layers, respectively. The flow is also affected by the surface tension $\sigma^{(2)}$ at the free surface, $y = h^{(2)}$, and the surface tension $\sigma^{(1)}$ at the interface between the layers, $y = h^{(1)}$.

The full Navier–Stokes system describing the flow includes the continuity equations and the momentum equations in both layers, and the following boundary conditions: no-slip and no-penetration of the first liquid at the wall, the kinematic conditions and the balance of shear and normal

Correspondence concerning this article should be addressed to: G. M. Sisoev at g.sisoev@bham.ac.uk.

stresses at the surface and interface taking into account capillary forces, and continuity of the velocity components is also stated at the interface. To state these equations and boundary conditions in dimensionless form, we use the scaling

$$t \to \frac{H_c}{\kappa U_c} t, \quad \left(x, y, h^{(1)}, h^{(2)}\right) \to H_c\left(\frac{x_\kappa}{\kappa}, y, h^{(1)}, h^{(2)}\right), \quad (u, v) \to U_c(u, \kappa v_\kappa), \quad p \to \rho^{(2)} U_c^2 p, \tag{1}$$

where t is time, u and v are the velocity components x and y directions, respectively, and p is the pressure. These relations include the film thickness of the waveless flow H_c as the length scale, the velocity scale U_c, and the stretching parameter κ defined below.

Then the governing equations and boundary conditions are rewritten in dimensionless form as follows

$$\frac{\partial u}{\partial x_\kappa} + \frac{\partial v_\kappa}{\partial y} = 0,$$

$$\frac{\partial u}{\partial t_\kappa} + u\frac{\partial u}{\partial x_\kappa} + v_\kappa \frac{\partial u}{\partial y} = -\frac{1}{\rho_0^{(j)}}\frac{\partial p}{\partial x_\kappa} + \frac{v_0^{(j)}}{\kappa \mathrm{Re}}\left(\kappa^2 \frac{\partial^2 u}{\partial x_\kappa^2} + \frac{\partial^2 u}{\partial y^2}\right) + \frac{1}{\kappa \mathrm{Fr}^2},$$

$$\kappa^2\left(\frac{\partial v_\kappa}{\partial t_\kappa} + u\frac{\partial v_\kappa}{\partial x_\kappa} + v_\kappa \frac{\partial v_\kappa}{\partial y}\right) = -\frac{1}{\rho_0^{(j)}}\frac{\partial p}{\partial y} + \frac{\kappa^2 v_0^{(j)}}{\kappa \mathrm{Re}}\left(\kappa^2 \frac{\partial^2 v_\kappa}{\partial x_\kappa^2} + \frac{\partial^2 v_\kappa}{\partial y^2}\right),$$

$$y = 0: \quad u = 0, \quad v_\kappa = 0,$$

$$y = h^{(1)}(x_\kappa, t_\kappa): \quad \frac{\partial h^{(1)}}{\partial t_\kappa} + u\frac{\partial h^{(1)}}{\partial x_\kappa} = v_\kappa, \quad [p_{nn}]_1^2 + \frac{\kappa^2 \sigma_0 \varsigma_\kappa^{(1)}}{\mathrm{We}} = 0,$$

$$[p_{n\tau}]_1^2 = 0, \quad [u]_1^2 = 0, \quad [v_\kappa]_1^2 = 0,$$

$$y = h^{(2)}(x_\kappa, t_\kappa): \quad \frac{\partial h^{(2)}}{\partial t_\kappa} + u\frac{\partial h^{(2)}}{\partial x_\kappa} = v_\kappa, \quad p_{nn} - \frac{\kappa^2 \varsigma_\kappa^{(2)}}{\mathrm{We}} = 0, \quad p_{n\tau} = 0. \tag{2}$$

Here the notation $[f]_1^2 \equiv f^{(2)} - f^{(1)}$ denotes the jump in quantity f from the value in the first liquid, $f^{(1)}$, to the value in the second one, $f^{(2)}$. The boundary conditions in (2) include the normal, p_{nn}, and tangential, $p_{n\tau}$, stresses, and the curvatures ς_κ which are calculated as follows

$$p_{nn}^{(j)} = -p^{(j)} + \frac{2\kappa^2 \rho_0^{(j)} v_0^{(j)}}{\kappa \mathrm{Re}}\left[1 + \kappa^2\left(\frac{\partial h^{(j)}}{\partial x_\kappa}\right)^2\right]^{-1} \times \left[\left(1 - \kappa^2\left(\frac{\partial h^{(j)}}{\partial x_\kappa}\right)^2\right)\frac{\partial v_\kappa^{(j)}}{\partial y} - \frac{\partial h^{(j)}}{\partial x_\kappa}\left(\frac{\partial u^{(j)}}{\partial y} + \kappa^2 \frac{\partial v_\kappa^{(j)}}{\partial x_\kappa}\right)\right],$$

$$p_{n\tau}^{(j)} = \frac{\rho_0^{(j)} v_0^{(j)}}{\mathrm{Re}}\left[1 + \kappa^2\left(\frac{\partial h^{(j)}}{\partial x_\kappa}\right)^2\right]^{-1} \times \left[\left(1 - \kappa^2\left(\frac{\partial h^{(j)}}{\partial x_\kappa}\right)^2\right)\left(\frac{\partial u^{(j)}}{\partial y} + \kappa^2 \frac{\partial v_\kappa^{(j)}}{\partial x_\kappa}\right) + 4\kappa^2 \frac{\partial h^{(j)}}{\partial x_\kappa}\frac{\partial v_\kappa^{(j)}}{\partial y}\right],$$

$$\varsigma_\kappa^{(j)} = \left[1 + \kappa^2\left(\frac{\partial h^{(j)}}{\partial x_\kappa}\right)^2\right]^{-\frac{3}{2}} \frac{\partial^2 h^{(j)}}{\partial x_\kappa^2}. \tag{3}$$

Equations 2 and 3 contain the following dimensionless parameters:

$$\mathrm{Re} = \frac{U_c H_c}{\nu^{(2)}}, \quad \mathrm{We} = \frac{\rho^{(2)} U_c^2 H_c}{\sigma^{(2)}}, \quad \mathrm{Fr}^2 = \frac{U_c^2}{g H_c},$$

$$\rho_0 = \frac{\rho^{(1)}}{\rho^{(2)}}, \quad \nu_0 = \frac{\nu^{(1)}}{\nu^{(2)}}, \quad \sigma_0 = \frac{\sigma^{(1)}}{\sigma^{(2)}},$$

where Re, We, and Fr are the Reynolds, Weber, and Froude numbers, respectively, and notations $\rho_0^{(1)} = \rho_0$, $\rho_0^{(2)} = 1$, $\nu_0^{(1)} = \nu_0$, and $\nu_0^{(2)} = 1$ have been used.

The problem (2) and (3) has a waveless solution with constant values of the first layer thickness $h^{(1)} = H$ and the film thickness $h^{(2)} = 1$ denoted by capital letters:

$$y \in [0, H]: \quad U^{(1)}(y) = \frac{\mathrm{Re}}{\nu_0 \mathrm{Fr}^2}\left(a^{(1)} y - \frac{y^2}{2}\right), \quad V^{(1)} = 0, \quad P^{(1)} = 0,$$

$$Q^{(1)} = \int_0^H U^{(1)} dy = \frac{\mathrm{Re} H^2}{2\nu_0 \mathrm{Fr}^2}\left[\frac{1}{\rho_0} + \left(\frac{2}{3} - \frac{1}{\rho_0}\right)H\right],$$

$$y \in [H, 1]: \quad U^{(2)}(y) = \frac{\mathrm{Re}}{\mathrm{Fr}^2}\left(a^{(2)} + y - \frac{y^2}{2}\right), \quad V^{(2)} = 0, \quad P^{(2)} = 0,$$

$$Q = \int_H^1 U^{(2)} dy = \frac{\mathrm{Re}(1-H)}{\mathrm{Fr}^2}\left[\frac{1}{3} + \left(\frac{1}{\rho_0 \nu_0} - \frac{2}{3}\right)H + \left(\frac{1}{3} + \frac{1}{2\nu_0} - \frac{1}{\rho_0 \nu_0}\right)H^2\right], \tag{4}$$

where

$$a^{(1)} = \frac{1}{\rho_0} + \left(1 - \frac{1}{\rho_0}\right)H, \quad a^{(2)} = \left(\frac{1+\nu_0}{2\nu_0} - \frac{1}{\rho_0 \nu_0}\right)H^2 + \left(\frac{1}{\rho_0 \nu_0} - 1\right)H.$$

Then the total flow rate in the film is

$$Q^{(2)} \equiv Q^{(1)} + Q = \frac{\varphi \mathrm{Re}}{\mathrm{Fr}^2},$$

where

$$\varphi = \frac{H^2}{2\nu_0}\left[\frac{1}{\rho_0} + \left(\frac{2}{3} - \frac{1}{\rho_0}\right)H\right] + (1-H)\left[\frac{1}{3} + \left(\frac{1}{\rho_0 \nu_0} - \frac{2}{3}\right)H + \left(\frac{1}{3} + \frac{1}{2\nu_0} - \frac{1}{\rho_0 \nu_0}\right)H^2\right].$$

We choose the average velocity in the waveless flow as the velocity scale U_c, and thus the dimensionless flow rate $Q^{(2)} = 1$, or $\mathrm{Fr}^2 = \varphi \mathrm{Re}$. The latter relation allows us to calculate the velocity scale $U_c = \varphi g H_c^2 / \nu^{(2)}$.

The stretching parameter κ is found from the fact that ordered capillary waves in liquid films are observed when there is a balance of gravity, viscosity and capillarity that can be written in the form $\kappa^2/\mathrm{We} = (\kappa \varphi \mathrm{Re})^{-1}$, and this relation leads to $\kappa = \left((45\delta)^2/\mathrm{Ka}^3\right)^{\frac{1}{11}}$. For most liquids, the Kapitza number is sufficiently large (e.g., $\mathrm{Ka} \approx 3000$ for water) which provides small values of κ^2 for real-life film flows.

Since $\mathrm{Fr}^2 = \varphi \mathrm{Re}$, we can exclude the Froude number form the list of independent parameters. In the film theory, it is also convenient to replace the Reynolds number and the

Weber number by the film parameter δ, and the Kapitza number Ka defined as

$$\delta \equiv \frac{1}{45\left(v^{(2)}\right)^2}\left(\frac{\rho^{(2)} g^4 H_c^{11}}{\sigma^{(2)}}\right)^{\frac{1}{3}}, \quad \mathrm{Ka} \equiv \frac{\sigma^{(2)}}{\rho^{(2)}\left(g\left(v^{(2)}\right)^4\right)^{\frac{1}{3}}}.$$

Neglecting terms of order $O(\kappa^2)$ in Eqs. 2 and 3, and taking into account the identity $\delta=\kappa\varphi \mathrm{Re}/5$ lead to the following simplified system

$$\frac{\partial u}{\partial x_\kappa}+\frac{\partial v_\kappa}{\partial y}=0,$$

$$\frac{\partial u}{\partial t_\kappa}+u\frac{\partial u}{\partial x_\kappa}+v_\kappa\frac{\partial u}{\partial y}=-\frac{1}{\rho_0^{(j)}}\frac{\partial p}{\partial x_\kappa}+\frac{\varphi v_0^{(j)}}{5\delta}\frac{\partial^2 u}{\partial y^2}+\frac{1}{5\delta},$$

$$\frac{\partial p}{\partial y}=0,$$

$$y=0: \quad u=0, \quad v_\kappa=0,$$

$$y=h^{(1)}(x_\kappa,t_\kappa): \quad \frac{\partial h^{(1)}}{\partial t_\kappa}+u\frac{\partial h^{(1)}}{\partial x_\kappa}=v_\kappa, \quad [u]_1^2=0, \quad [v_\kappa]_1^2=0,$$

$$\left[\rho_0^{(j)} v_0^{(j)}\frac{\partial u}{\partial y}\right]_1^2=0, \quad [-p]_1^2+\frac{\sigma_0}{5\delta}\frac{\partial^2 h^{(1)}}{\partial x_\kappa^2}=0,$$

$$y=h^{(2)}(x_\kappa,t_\kappa): \quad \frac{\partial h^{(2)}}{\partial t_\kappa}+u\frac{\partial h^{(2)}}{\partial x_\kappa}=v_\kappa, \quad \frac{\partial u}{\partial y}=0, \quad p+\frac{1}{5\delta}\frac{\partial^2 h^{(2)}}{\partial x_\kappa^2}=0. \tag{5}$$

From the y-momentum equations and the boundary conditions for the normal stresses, we find the pressures in the layers

$$p^{(1)}=-\frac{1}{5\delta}\left(\sigma_0\frac{\partial^2 h^{(1)}}{\partial x_\kappa^2}+\frac{\partial^2 h^{(2)}}{\partial x_\kappa^2}\right), \quad p^{(2)}=-\frac{1}{5\delta}\frac{\partial^2 h^{(2)}}{\partial x_\kappa^2}.$$

These formulas allow us to eliminate the pressure from the x-momentum equations in 5.

Similar to the case of the single-layer film, we approximate the velocity profiles with the parabolic functions

$$y\in\left[0,h^{(1)}\right]: \quad u=U_{11}y+U_{12}y^2,$$

$$U_{12}=\frac{3}{h^{(1)}[(3-4\rho_0 v_0)h^{(1)}+4\rho_0 v_0 h^{(2)}]}$$

$$\times\left\{\frac{3q^{(2)}}{h^{(2)}-h^{(1)}}-\left[\frac{3}{h^{(2)}-h^{(1)}}+\frac{2}{\left(h^{(1)}\right)^2}\left[(3-\rho_0 v_0)h^{(1)}+\rho_0 v_0 h^{(2)}\right]\right]q^{(1)}\right\},$$

$$U_{11}=\frac{2q^{(1)}}{\left(h^{(1)}\right)^2}-\frac{2h^{(1)}U_{12}}{3},$$

$$y\in\left[h^{(1)},h^{(2)}\right]: \quad u=U_{20}+U_{22}\left(y^2-2h^{(2)}y\right),$$

$$U_{22}=-\frac{\rho_0 v_0}{2}\frac{U_{11}+2U_{12}h^{(1)}}{h^{(2)}-h^{(1)}},$$

$$U_{20}=\frac{q^{(2)}-q^{(1)}}{h^{(2)}-h^{(1)}}+\frac{1}{3}\left[2\left(h^{(2)}\right)^2+2h^{(1)}h^{(2)}-\left(h^{(1)}\right)^2\right]U_{22}$$

satisfying the boundary conditions for the velocity component u. Here the local flow rates in the first layer and the film

$$q^{(1)}(x_\kappa,t_\kappa)\equiv\int_0^{h^{(1)}}u^{(1)}dy, \quad q^{(2)}(x_\kappa,t_\kappa)\equiv q^{(1)}+\int_{h^{(1)}}^{h^{(2)}}u^{(2)}dy$$

have been used. The velocity profiles are reduced to the exact solution (4) in the case of the waveless flow.

Integrating the continuity equations and the momentum equations across each layer leads to the following evolution system

$$\frac{\partial h^{(1)}}{\partial t_\kappa}+\frac{\partial q^{(1)}}{\partial x_\kappa}=0,$$

$$\frac{\partial q^{(1)}}{\partial t_\kappa}+\frac{\partial J^{(1)}}{\partial x_\kappa}=\frac{h^{(1)}}{5\delta}\left(\frac{\sigma_0}{\rho_0}\frac{\partial^3 h^{(1)}}{\partial x_\kappa^3}+\frac{1}{\rho_0}\frac{\partial^3 h^{(2)}}{\partial x_\kappa^3}+2\varphi v_0 U_{12}+1\right),$$

$$\frac{\partial h^{(2)}}{\partial t_\kappa}+\frac{\partial q^{(2)}}{\partial x_\kappa}=0,$$

$$\frac{\partial q^{(2)}}{\partial t_\kappa}+\frac{\partial J^{(2)}}{\partial x_\kappa}=\frac{1}{5\delta}\left[\frac{\sigma_0 h^{(1)}}{\rho_0}\frac{\partial^3 h^{(1)}}{\partial x_\kappa^3}+\left(h^{(2)}+\left(\frac{1}{\rho_0}-1\right)h^{(1)}\right)\frac{\partial^3 h^{(2)}}{\partial x_\kappa^3}\right.$$
$$\left.+\varphi\left[2v_0U_{12}h^{(1)}(1-\rho_0)-\rho_0 v_0 U_{11}\right]+h^{(2)}\right], \tag{6}$$

where the functions

$$J^{(1)}=\left(h^{(1)}\right)^3\left[\frac{U_{11}^2}{3}+\frac{U_{11}U_{12}}{2}h^{(1)}+\frac{U_{12}^2}{5}\left(h^{(1)}\right)^2\right],$$

$$J^{(2)}=J^{(1)}+U_{20}^2\left(h^{(2)}-h^{(1)}\right)-2U_{20}U_{22}h^{(2)}\left[\left(h^{(2)}\right)^2-\left(h^{(1)}\right)^2\right]$$
$$+\frac{2}{3}\left[2U_{22}^2\left(h^{(2)}\right)^2+U_{20}U_{22}\right]\left[\left(h^{(2)}\right)^3-\left(h^{(1)}\right)^3\right]$$
$$-U_{22}^2h^{(2)}\left[\left(h^{(2)}\right)^4-\left(h^{(1)}\right)^4\right]+\frac{U_{22}^2}{5}\left[\left(h^{(2)}\right)^5-\left(h^{(1)}\right)^5\right]$$

have been introduced.

Properties of the model (6) are analyzed in Ref. 27. The limitations under which the model is derived are the following: small value of the stretching parameter for specific values of the similarity parameters δ, ρ_0, v_0, and σ_0, and the assumption about parabolic character of velocity profiles in both layers. To verify the model (6), linear stability analysis of the waveless flow (4) has been carried out and compared with the unstable modes computed in Ref. 22 for the Orr-Sommerfeld problem. It has been shown that the model provides a good approximation of the full Navier-Stokes problem for a wide range of the similarity parameters.

Regular waves

In this study, we consider the gas absorption in regimes of steady-traveling space-periodic waves of constant velocity and shape: $h^{(1)}(\eta), h^{(2)}(\eta), q^{(1)}(\eta), q^{(2)}(\eta)$ where $\eta=\alpha_\kappa(x_\kappa-ct_\kappa)$, c is the wave velocity and α_κ is the wavenumber.

Equations (6) lead to the following eigenvalue problem for the first layer thickness $h^{(1)}(\eta)$, the film thickness $h^{(2)}(\eta)$ and the wave velocity c. The eigenvalue problem includes the sixth order system of differential equations

$$-c^2\frac{dh^{(1)}}{d\eta}+\frac{dJ^{(1)}}{d\eta}=\frac{h^{(1)}}{5\delta\alpha_\kappa}\left(\frac{\alpha_\kappa^3\sigma_0}{\rho_0}\frac{d^3h^{(1)}}{d\eta^3}+\frac{\alpha_\kappa^3}{\rho_0}\frac{d^3h^{(2)}}{d\eta^3}+2\varphi v_0U_{12}+1\right),$$

$$-c^2\frac{dh^{(2)}}{d\eta}+\frac{dJ^{(2)}}{d\eta}=\frac{\alpha_\kappa^2}{5\delta}\left[\frac{\sigma_0h^{(1)}}{\rho_0}\frac{d^3h^{(1)}}{d\eta^3}+\left(h^{(2)}+\left(\frac{1}{\rho_0}-1\right)h^{(1)}\right)\frac{d^3h^{(2)}}{d\eta^3}\right]$$
$$+\frac{\varphi}{5\delta\alpha_\kappa}\left[2v_0U_{12}h^{(1)}(1-\rho_0)-\rho_0v_0U_{11}\right]+\frac{h^{(2)}}{5\delta\alpha_\kappa} \tag{7}$$

accompanied by periodic boundary conditions

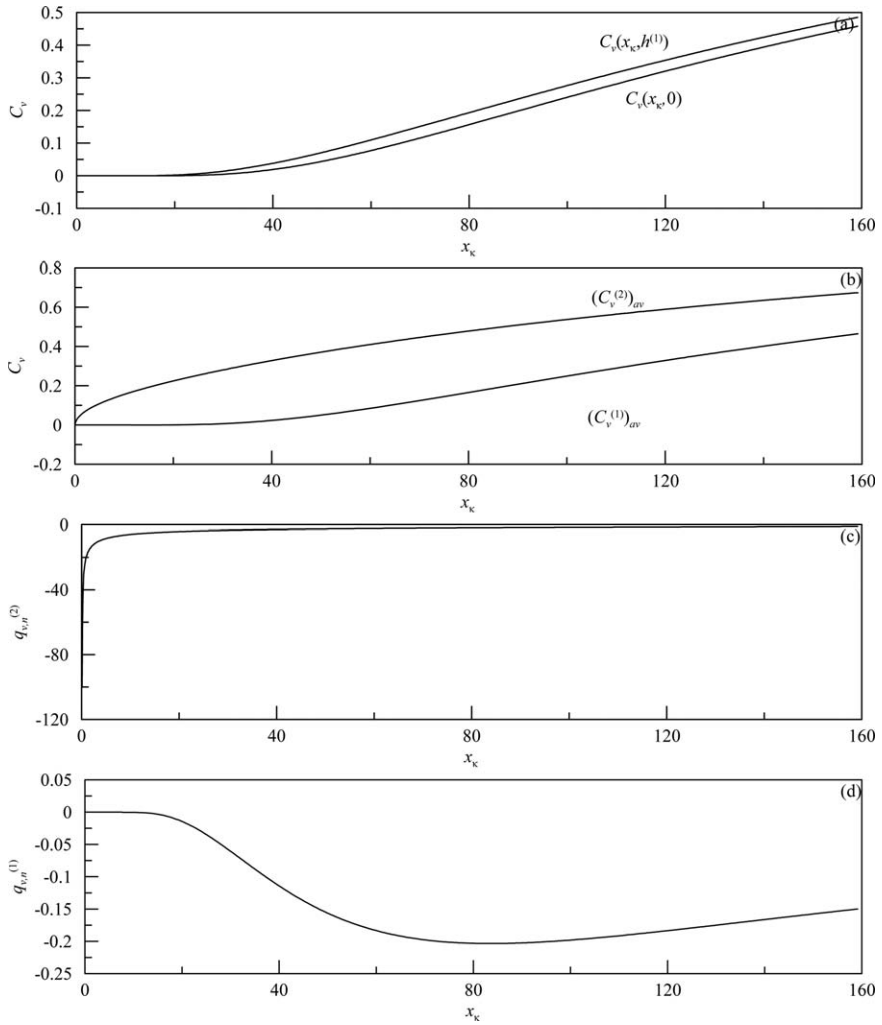

Figure 1. The interface and wall concentrations (a), the average concentrations in the layers (b), the local fluxes at the surface (c), and interface (d) for the waveless flow at $H = 0.3$.

$$h^{(1)}\Big|_0 = h^{(1)}\Big|_{2\pi}, \quad \frac{dh^{(1)}}{d\eta}\Big|_0 = \frac{dh^{(1)}}{d\eta}\Big|_{2\pi}, \quad \frac{d^2h^{(1)}}{d\eta^2}\Big|_0 = \frac{d^2h^{(1)}}{d\eta^2}\Big|_{2\pi},$$
$$h^{(2)}|_0 = h^{(2)}\Big|_{2\pi}, \quad \frac{dh^{(2)}}{d\eta}\Big|_0 = \frac{dh^{(2)}}{d\eta}\Big|_{2\pi}, \quad \frac{d^2h^{(2)}}{d\eta^2}\Big|_0 = \frac{d^2h^{(2)}}{d\eta^2}\Big|_{2\pi}. \tag{8}$$

The invariance of a solution to a shift along the η-axis completes the eigenvalue problem.

In the class of space-periodic solutions, integrating the continuity equations in (6) with respect to x_κ over the space period $2\pi/\alpha_\kappa$ shows that the average thicknesses $h_0^{(1)}$ and $h_0^{(2)}$ do not depend on time, and thus these variables are equal to their values in the steady waveless flow: $h_0^{(1)} = H$ and $h_0^{(2)} = 1$.

Similar to the case of the single layer film, the eigenvalue problem for the two-layer film possesses a rich set of solutions. In particular, there is nonuniqueness of solutions when two or more solutions are at given values of the similarity parameters ρ_0, ν_0, σ_0, δ and H, and the wavenumber α_κ. To select solutions suitable for comparison with experimental data, we apply the concept of so-called dominating waves revealed in Ref. 26 where it was shown that in most cases the developed wave regimes are oscillating wavy flows in neighborhoods of steady-traveling waves with maximum velocity and amplitude among all steady-traveling space-periodic waves at given wavenumber α_κ, or the normalized wavenumber $s = \alpha_\kappa/\alpha_{\kappa,n}$ where $\alpha_{\kappa,n}$ is the neutral

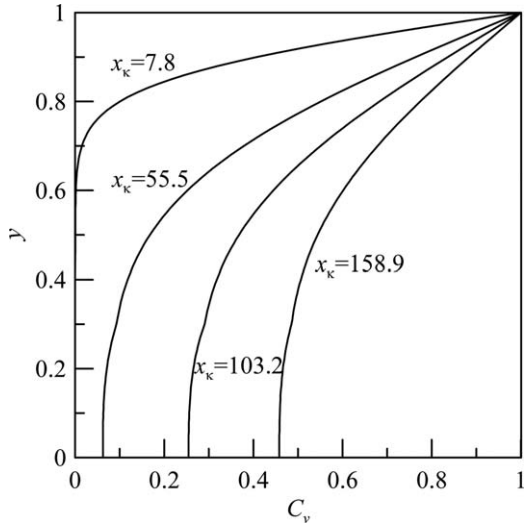

Figure 2. Instant profiles of the gas concentration in the case shown in Figure 1.

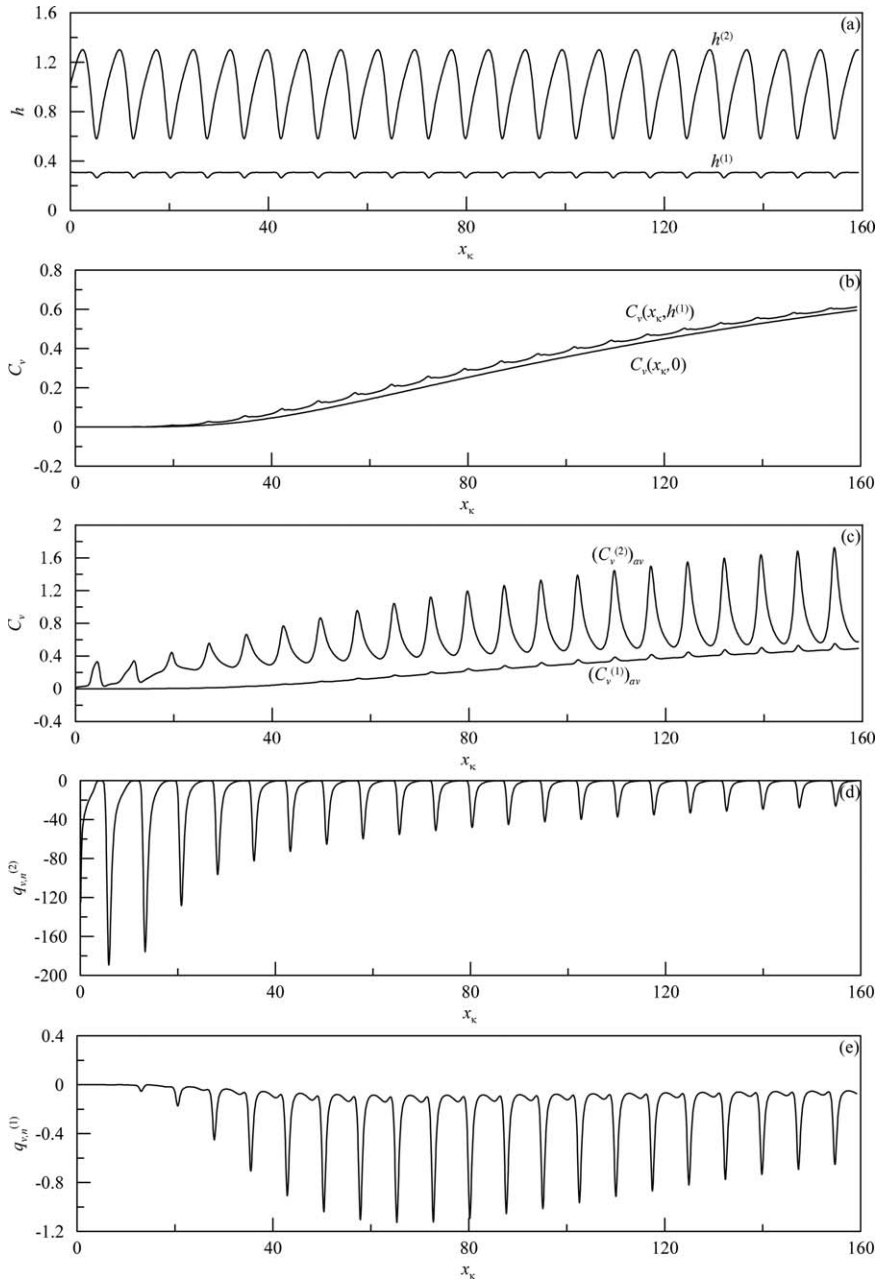

Figure 3. Instant profiles of the interface and surface (a), the interface and wall concentrations (b), the average concentrations in the layers (c), the local flux at the surface (d), and interface (e) for the dominating wave at $s = 0.6$ and $H = 0.3$.

wavenumber. The film surface of a dominating wave does not change its shape, and the interface demonstrates small-amplitude oscillations for most values of the similarity parameters and wavenumbers except the parameters in neighborhoods of bifurcation points. Below we use the attracting steady-traveling waves to compute absorption in a two-layer falling film.

Mass Transfer

Absorption of a weakly soluble gas into a two-layer film flowing down a vertical plane is governed by convective-diffusion equations for the gas concentration in both layers. The equations are accompanied by boundary conditions including a given constant gas concentration $C_{v,s}$ at the free surface, absence of the gas flux through the wall, continuity of the gas concentration and normal gas flux at the interface. To solve the diffusion problem, we also have to state inlet and outlet conditions at two cross sections along the x_κ axis. The full diffusion problem can be rewritten in a dimensionless form using (1) accompanied by the replacement $C_v \rightarrow C_{v,s}C_v$.

In the framework of the hydrodynamical approximate model, and taking into account large values of the Schmidt number $\mathrm{Sc}=\nu^{(2)}/D_v^{(2)}$, where $D_v^{(2)}$ is the Fick's law diffusion coefficient in the second layer, we can reduce the full diffusion problem to its long-wave approximation.[1]

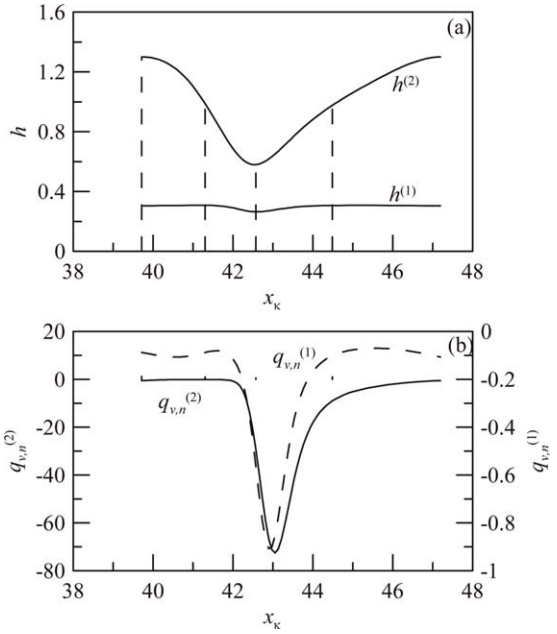

Figure 4. Instant profiles of the interface and surface (a) and the local fluxes (b) at the inlet area in the case shown Figure 3.

$$\frac{\partial C_v}{\partial t_\kappa}+u\frac{\partial C_v}{\partial x_\kappa}+v_\kappa\frac{\partial C_v}{\partial y}=\frac{D_0^{(j)}}{\kappa \mathrm{ScRe}}\frac{\partial^2 C_v}{\partial y^2},$$

$$y=0: \quad \frac{\partial C_v}{\partial y}=0,$$

$$y=h^{(1)}(x_\kappa,t_\kappa): \quad [C_v]_1^2=0, \quad [q_{v,n}]_1^2=0, \tag{9}$$

$$y=h^{(2)}(x_\kappa,t_\kappa): \quad C_v=C_{v,s},$$

$$x_\kappa=L_{\kappa,l}: \quad C_v=C_{v,l}(y,t_\kappa),$$

where $q_{v,n}=-D_0^{(j)}\frac{\partial C_v}{\partial y}, D_0^{(2)}=1$ and $D_0^{(1)}=D_v^{(1)}/D_v^{(2)}, D_v^{(1)}$ is the Fick's law diffusion coefficient in the first layer. In this approximation, we omit the terms of $O(\kappa^2)$ in equations and boundary conditions to maintain consistency with the thin layer approximation used to derive Eqs. 5. We note that the outlet boundary condition is not stated in the long-wave approximation.

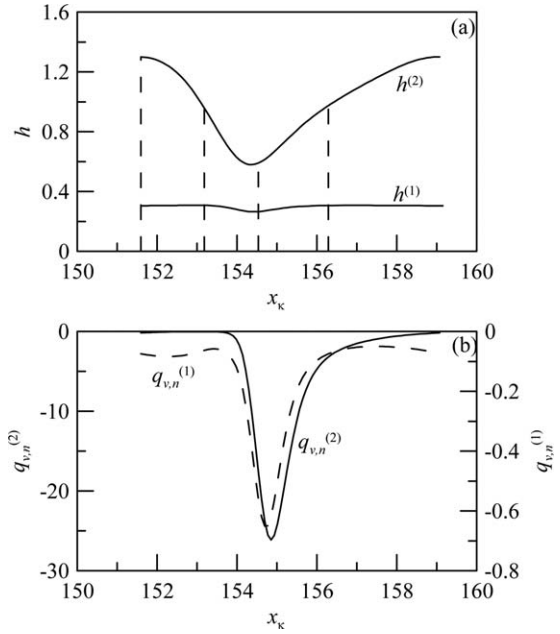

Figure 6. Instant profiles of the interface and surface (a) and the local fluxes (b) in the outlet area in the case shown Figure 3.

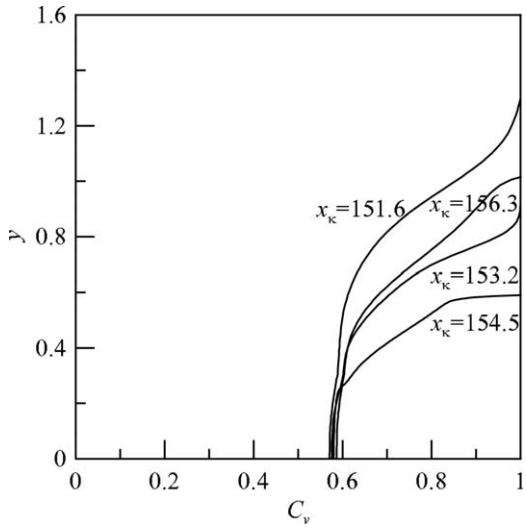

Figure 7. Instant profiles of concentration in the outlet area in the case shown Figure 3.

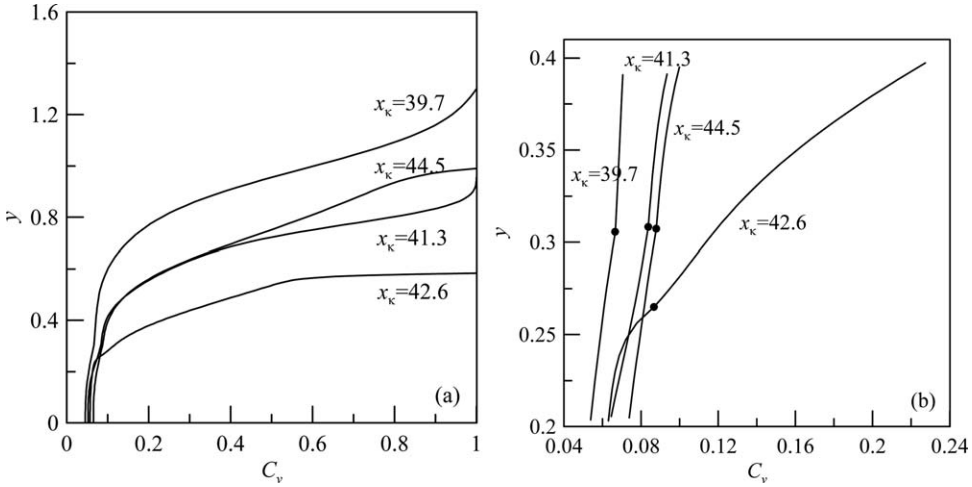

Figure 5. Global (a) and local (b) instant profiles of concentration at the inlet area in the case shown Figure 3.

To characterize the intensity of the gas absorption, we use the integral mass fluxes through the interface and the surface

$$Q_{v,n}^{(1)}=-\frac{D_0^{(1)}}{\kappa}\int_{L_{\kappa,l}}^{L_{\kappa,r}}\frac{\partial C_v}{\partial y}\Big|_{y=h^{(1)}-0}dx_\kappa,\quad Q_{v,n}^{(2)}=-\frac{D_0^{(2)}}{\kappa}\int_{L_{\kappa,l}}^{L_{\kappa,r}}\frac{\partial C_v}{\partial y}\Big|_{y=h^{(2)}-0}dx_\kappa,$$

and the average concentrations in the layers:

$$\left(C_v^{(1)}\right)_{av}=\frac{1}{h^{(1)}}\int_0^{h^{(1)}}C_v^{(1)}dy,\quad \left(C_v^{(2)}\right)_{av}=\frac{1}{h^{(2)}-h^{(1)}}\int_{h^{(1)}}^{h^{(2)}}C_v^{(2)}dy.$$

Results

Computations have been carried out for absorption of carbon dioxide into a film consisting of water as the first liquid and benzene as the second liquid. In this case the similarity parameters of the model are $\rho_0=1.14, \nu_0=1.36,\ \sigma_0=1.16,$ $D_0=0.55,$ Sc$=231$, and we consider the case $\delta=0.1$.

We start from the case when the inlet flow does not contain gas. First, we compute gas absorption into a waveless falling film. Then we model the absorption in regimes of the dominating waves described by the Eqs. 7 and 8.

To demonstrate the role of wave regimes depending on the wavenumber, we present results in two cases at $H=0.3$. Then, we show the role of the average thickness of the first flow in the case $H=0.6$.

We also solve the absorption problem in the case when the inlet gas concentration in the first layer and second layer are $C_{v,l}^{(1)}=1$ and $C_{v,l}^{(2)}=0$, respectively.

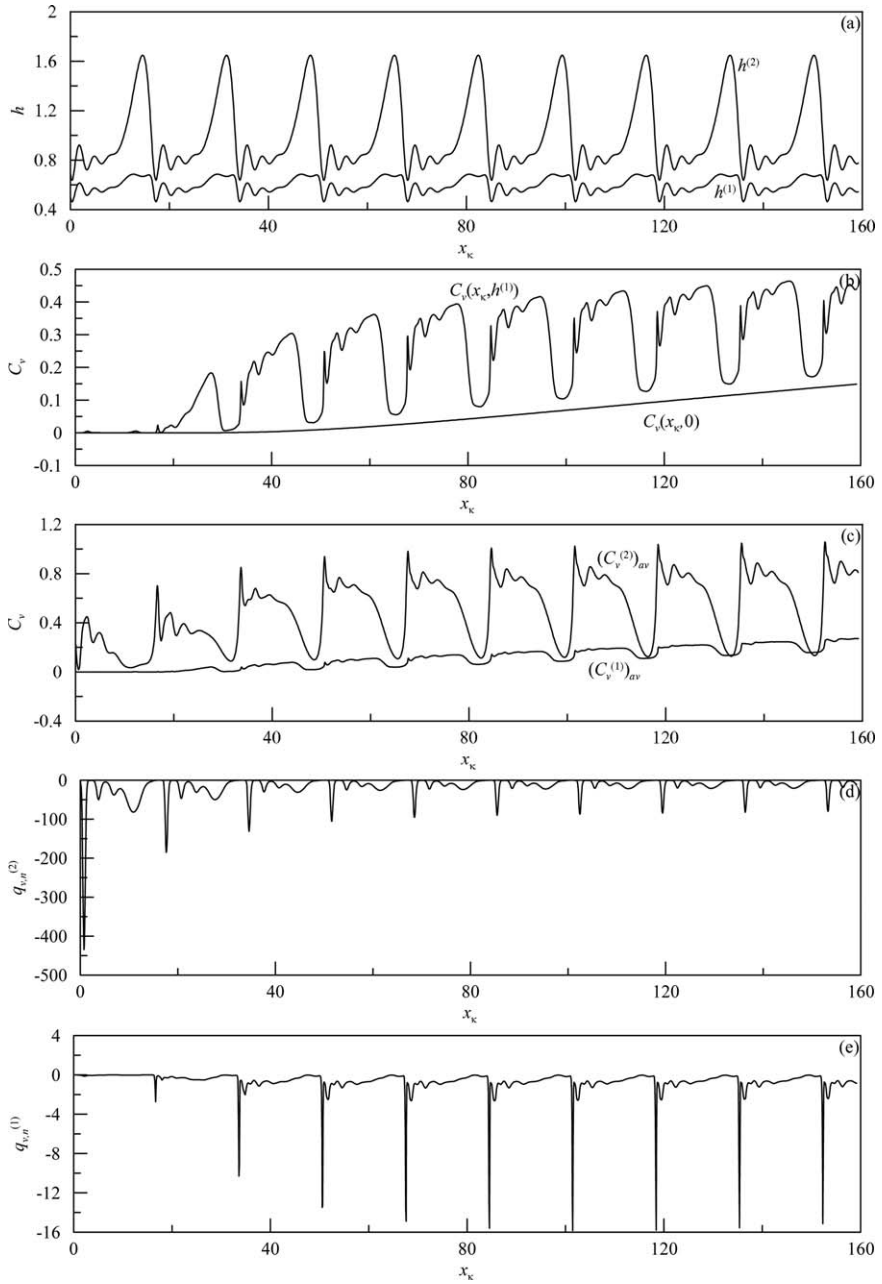

Figure 8. Instant profiles of the interface and surface (a), the interface and wall concentrations (b), the average concentrations in the layers (c), the local flux at the surface (d), and interface (e) for dominating wave at $s=0.3$ and $H=0.3$.

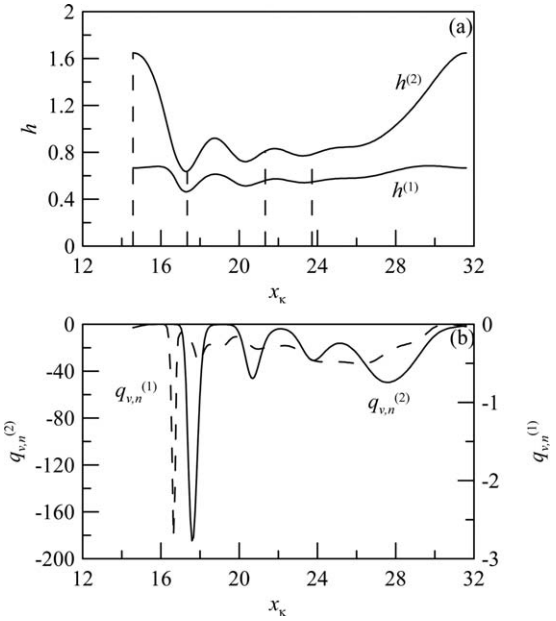

Figure 9. Instant profiles of the interface and surface (a) and the local fluxes (b) at the inlet area in the case Figure 8.

Absorption in regimes of dominating waves at H = 0.3

Absorption in the Waveless Flow. Figure 1 shows the functions characterizing the absorption in the waveless flow at $H = 0.3$. The concentrations at the interface $C_v\left(x_\kappa, h^{(1)}\right)$, and the wall $C_v(x_\kappa,0)$, shown in panel (a), are zero at the inlet region and then monotonically increase downstream. Behavior of the average concentrations in the layers, see panel (b), is different: the concentration in the second layer increases from $x_\kappa = 0$, and the first layer concentration is equal to zero at the inlet region.

The role of the inlet region also affects the local fluxes through the film surface and interface. The modulus of the local flux at the surface, $q_{v,n}^{(2)}$, shown in panel (c) decreases downstream since the convective flux of the gas along the x_κ-axis flattens the concentration gradient at the surface. As noted above, the gas concentration at the interface, panel (d), is zero at the inlet region where the diffusion boundary layer has not reached the interface. With further increasing x_κ, the interface becomes located inside this diffusion boundary layer and the modulus of the flux, $q_{v,n}^{(1)}$, grows. Then, the gas concentration within the first layer increases, and the concentration profiles in the neighborhood of the interface flatten and the value $|q_{v,n}^{(1)}|$ decreases. The concentration profiles given in Figure 2 shows how the diffusion boundary layer is developing.

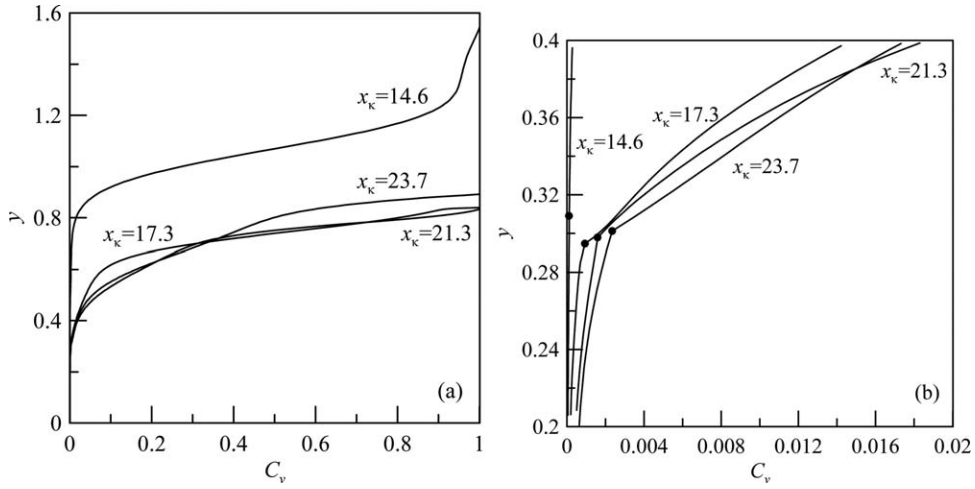

Figure 10. Global (a) and local (b) instant profiles of concentration in the inlet area in the case Figure 8.

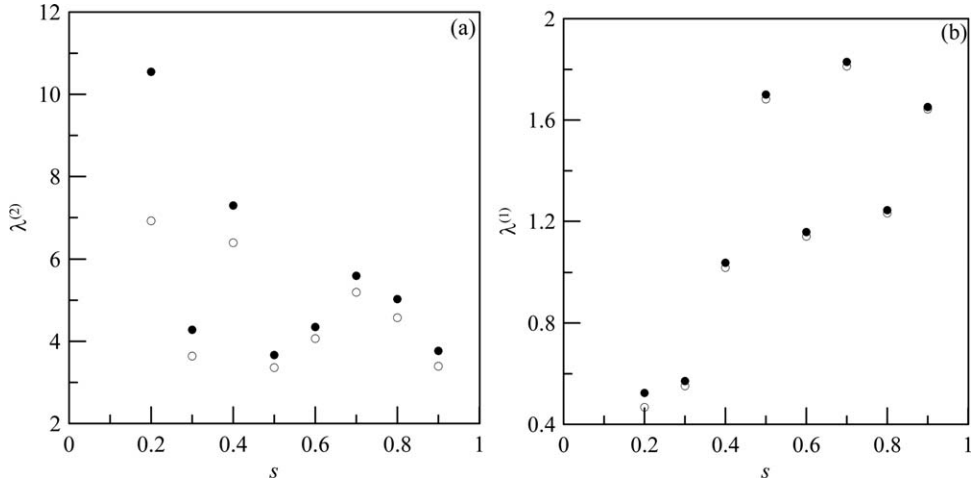

Figure 11. Minimum and maximum values of $\lambda^{(2)}$ (a) and $\lambda^{(1)}$ (b) denoted by empty and full circles, respectively, at $H = 0.3$.

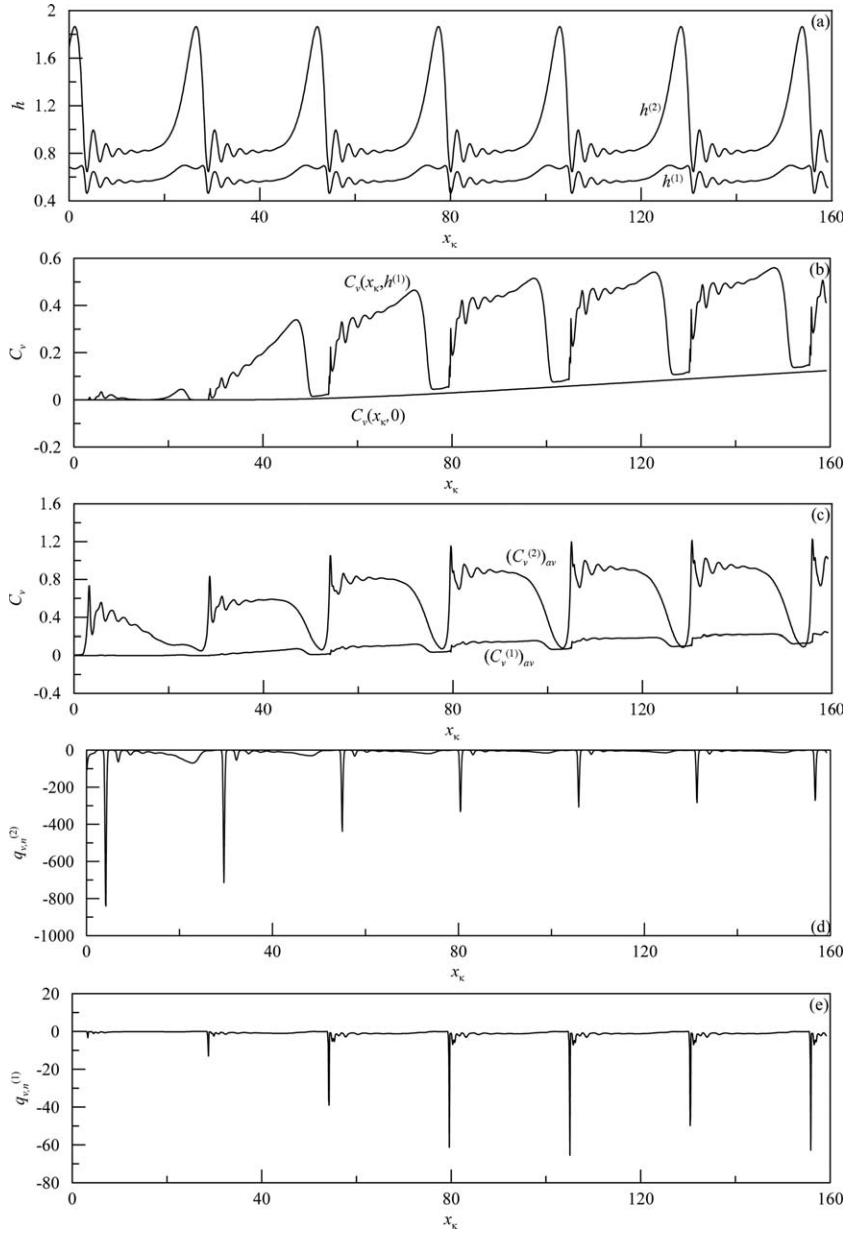

Figure 12. Instant profiles of the interface and surface (a), the interface and wall concentrations (b), the average concentrations in the layers (c), the local flux at the surface (d), and interface (e) at $H = 0.6$ and $s = 0.2$.

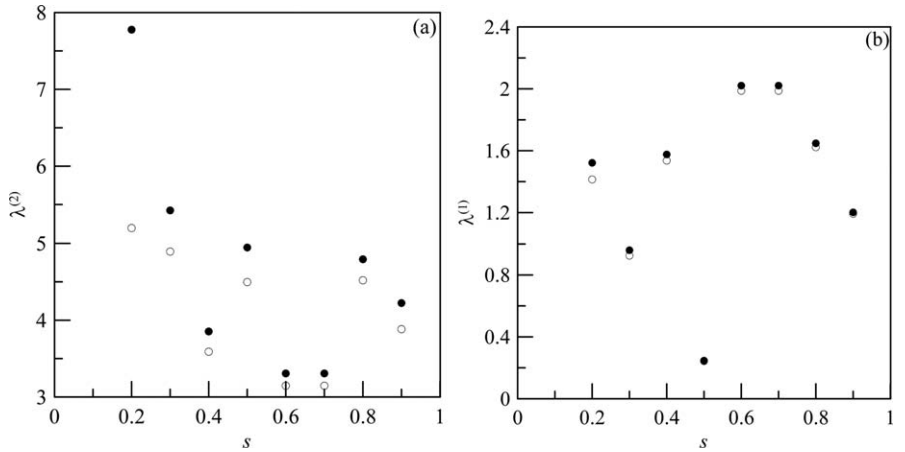

Figure 13. Minimum and maximum values of $\lambda^{(2)}$ (a) and $\lambda^{(1)}$ (b) denoted by empty and full circles, respectively, at $H = 0.6$.

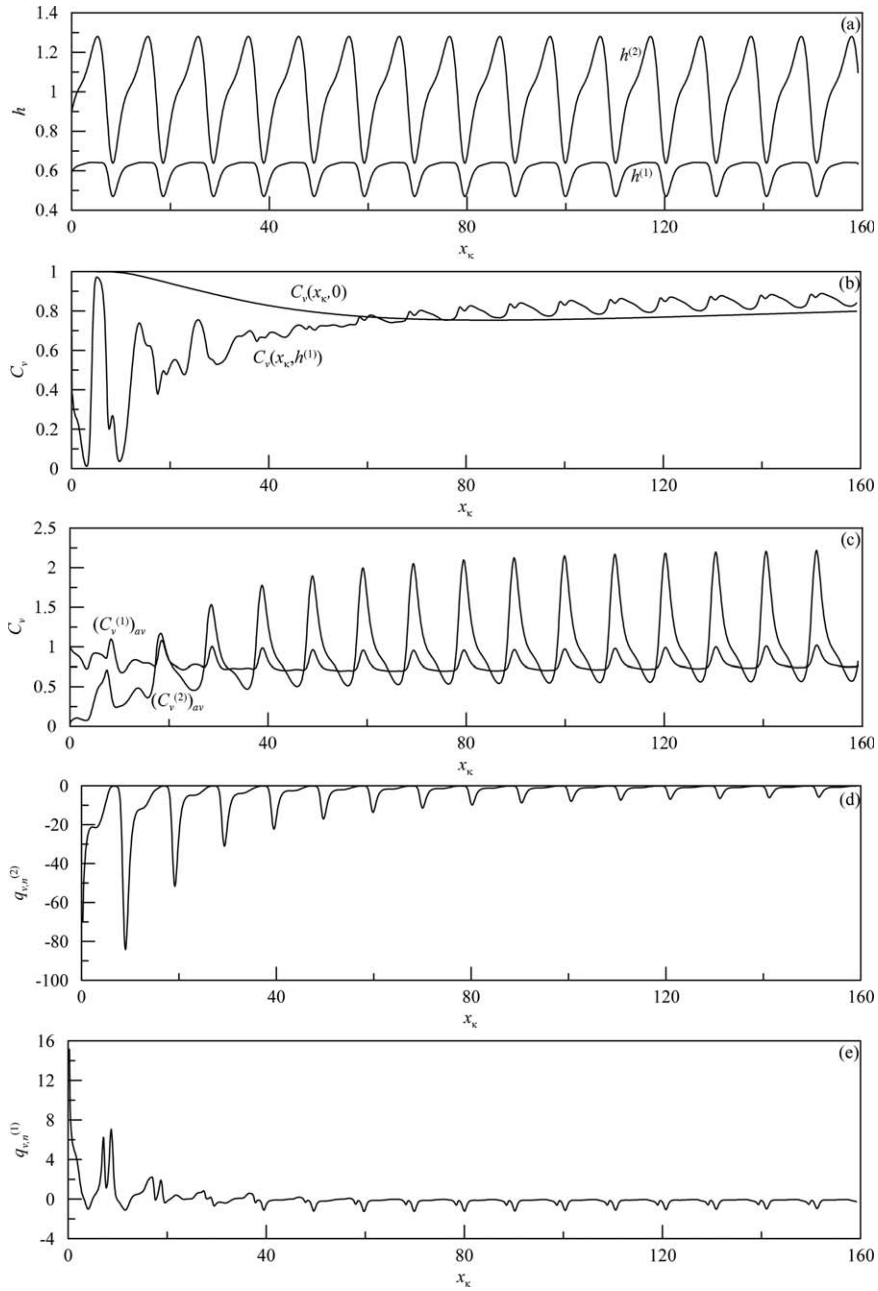

Figure 14. Instant profiles of the interface and surface (a), the interface and wall concentrations (b), the average concentrations in the layers (c), the local flux at the surface (d), and interface (e) at $H = 0.6$ and $s = 0.5$ at the inlet conditions with $C_v^{(1)}(0,y)=1, C_v^{(2)}(0,y)=0$.

Dominating Wave Regimes at s = 0.6. Figure 3 shows instant thicknesses of the film and the first layer, panel (a), and concentration parameters on longitudinal coordinate x_κ at $H = 0.3$ in the case of the dominating wave at $s = 0.6$.

Similar to the absorption into the waveless flow, the wall concentration, panel (b), is zero over the inlet region, and then it monotonically increases downstream. Conversely, the gas concentration on the interface increases downstream with oscillations.

In contrast to the waveless flow, the average gas concentrations in both layers are increasing with oscillations. We note that the amplitude of oscillations of this parameter in the second layer is greater than the one in the first layer. This can be explained by the larger amplitude of the surface waves compared with the interface waves.

The local fluxes at the surface and interface are given in panels (d) and (e), respectively. Similar to the case of the waveless flow, intensity of mass transfer on the surface decreases, and the intensity on the interface initially increases and then begins to slowly decrease.

Figure 4a shows the local shapes of the surface and interface at the inlet area in the case shown in Figure 3a, and distributions of the local gas fluxes at the surface and the interface are shown in Figure 4b. It is seen that the mass transfer through the interface is relatively small in comparison with the mass transfer through the film surface. The concentration profiles in the inlet area corresponding to the case in Figure 4 are shown in Figure 5. It can be said that when the layers have almost minimum thicknesses at $x_\kappa = 42.6$, the concentration gradient and modules of the fluxes are highest.

Figure 6a shows the local profiles of the surface and interface in the outlet area corresponding to Figure 3, and panel Figure 6b demonstrates the distribution of the gas fluxes along the wave. In the outlet area, the local flux at the interface is also smaller than at the surface. Figure 7 demonstrates the concentration profiles in the outlet area. It is seen that the concentration here is higher than the inlet area, see Figures 5 and 7. Locally, the concentration gradient, as in the previous case, is largest at minimum thicknesses of the layers.

Dominating Wave Regimes at s = 0.3. To analyze gas absorption at dominating wave at $s = 0.3$, we have again plotted profiles concentrations and fluxes in Figure 8. Comparing the profile of Figure 8 to that of Figure 3, panels (a), we see that the waves exhibit intermediate oscillations. This leads to very different behavior of the wall and interface concentrations, see Figure 8b, and also the average concentrations in the layers, see Figure 8c. The local fluxes at the surface and interface have large isolated peaks, and compared with Figure 3, occur with decreased frequency.

Figure 9 shows that in contrast to the case $s = 0.6$ there are a few local maximums of the values $|q_{v,n}^{(2)}|$ and $|q_{v,n}^{(1)}|$ in the case $s = 0.3$.

As previously, the largest absolute values of the fluxes correspond to local minima of the thicknesses of the first layer and film, see Figure 10.

Figure 11 shows minimum and maximum values of $\lambda^{(2)} = Q_{v,n}^{(2)}/Q_{v,n,0}^{(2)}$ and $\lambda^{(1)} = Q_{v,n}^{(1)}/Q_{v,n,0}^{(1)}$ at different wavenumbers for $H = 0.3$ where subscript 0 denotes values corresponding to the waveless flow. We can see nonlinear dependence of $\lambda^{(2)}$ and $\lambda^{(1)}$ on the wavenumber s, and this is similar to the case of the single-layer film.[1,5]

Absorption in regimes of dominating waves at H = 0.6

No Inlet Gas. To demonstrate the effects of the layer thicknesses, Figure 12 corresponding to the dominating wave at $s = 0.2$. It is seen that in all panels of Figure 12, there are solitary-like oscillations of all parameters, for example, the

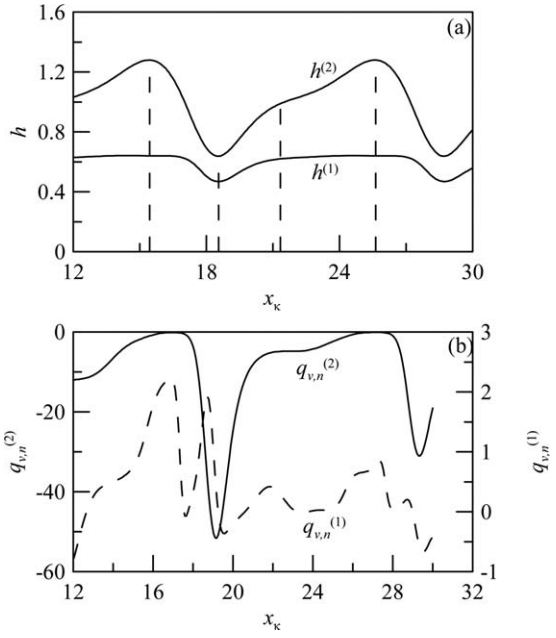

Figure 15. Instant profiles of the interface and surface (a) and the local fluxes (b) at the inlet area in the case shown in Figure 14.

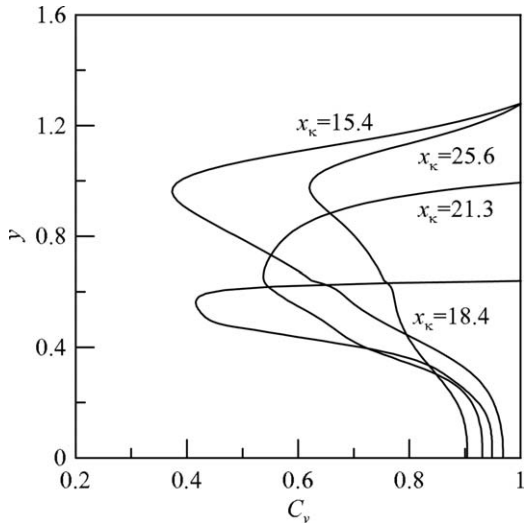

Figure 16. Instant profiles of concentration at the inlet area in the case shown in Figure 14.

wall and interface concentrations, the average concentrations in both layers. In particular, it is relevant to the local fluxes at the surface and interface shown in Figures 12d, e.

Figure 13 summarizes the intervals of oscillations of values of $\lambda^{(2)}$ and $\lambda^{(1)}$ at the surface and interface, respectively, for different wavenumbers at $H = 0.6$. Again, there are nonlinear dependencies of these coefficients on the wavenumber s.

Different Inlet Gas Concentrations in the Layers. To analyze the role of the inlet conditions at $x_\kappa = 0$, absorption in the steady-traveling wave regime at $s = 0.5$ in the case $H = 0.6$ and the inlet conditions $C_v^{(1)}(0, y) = 1, C_v^{(2)}(0, y) = 0$ is shown in Figure 14. In Figure 14a, while the surface profile is similar to Figure 3a, the amplitude of the interface waves is larger. Unlike the previously discussed cases, the gas concentration at wall interface decreases, and the interface concentration increases until saturation begins, see Figure 14b. It is seen in Figure 14c that the average concentrations in the layers overlap. The local fluxes at the surface and interface are smaller than the other cases, see Figures 14d, e.

Comparing with Figure 9a, there are no small oscillations at the inlet area neither in the surface nor interface in Figure 15a. Different from the other cases, see Figures 4b and 9b, the local fluxes of the layers at the inlet area do not imitate each other, see Figure 15b.

The concentration of gas at the inlet area decreases first and then increases dramatically for different values of x_κ shown in Figure 16.

Conclusions

The mass-transfer problem in a two-layer film flowing down a vertical plane has been formulated and solved for the first time. The analysis is based on an approximate long-wave model generalizing the Kapitza–Shkadov model for a single-layer film. Nonlinear wavy regimes in the two-layer film flow have been computed and the absorption problem has been solved numerically.

It has been shown that, similar to the single-film flow, the absorption rate is increased for wavy regimes in comparison with the waveless flow, and this amplification takes place at the interface between the liquid as well as at the film surface. Numerous transient computations have demonstrated

that the growth of the absorption rate is explained by the nonuniform distribution of the concentration gradient along the film surface and the interface. The largest gradients and thus largest local gas fluxes at the surface and interface are observed at wave troughs where thicknesses of the first layer and the whole film are minimum.

The suggested algorithm for computing the gas absorption into a two-layer falling film contains two steps: computing the hydrodynamical problem for the evolution equations and then solving the diffusion problem. Reducing the full Navier–Stokes problem to the evolution equations provides a considerable progress to save computational resources to carry out systematic numerical experiments to find optimized regimes of absorption. Moreover, as well as in the case of a single-layer film, the algorithm can be generalized for other types of two-layer flow, for example, flows over a spinning disk.

Literature Cited

1. Sisoev GM, Matar OK, Lawrence CJ. Absorption of gas into a wavy falling film. *Chem Eng Sci*. 2005;60:827–838.
2. Sisoev GM, Matar OK, Lawrence CJ. Gas absorption into a wavy film flowing over a spinning disc. *Chem Eng Sci*. 2005;60:2049–2058.
3. Kholpanov LP, Shkadov VYa. *Hydrodynamics and Heat and Mass Transfer at Interfaces*. Moscow: Nauka, 1990.
4. Killion JD, Garimella S. A critical review of models of coupled heat and mass transfer in falling-film absoption. *Int J Refrigeration*. 2001;24:755–797.
5. Rastaturin AA, Demekhin EA, Kalaidin EN. Optimal regimes of mass transfer in fluid films. *Doklady Phys*. 2005;50(2):115–117.
6. Albert C, Marschall H, Bothe D. Direct numerical simulation of interfacial mass transfer into falling films. *Int J Heat Mass Transfer*. 2014;69:343–357.
7. Hu J, Yang X, Yu J, Dai G. Numerical simulation of carbon dioxide (CO_2) absorption and interfacial mass transfer across vertically wavy falling film. *Chem Eng Sci*. 2014;116:243–243.
8. Kapitza PL, Kapitza SP. Wave flow of thin viscous liquid films. III. Experimental study of wave regime of a flow. *J Exp Theor Phys*. 1949;19(2):105–120.
9. Shkadov VYa. Wave flow regimes of a thin layer of viscous fluid subject to gravity. *Fluid Dyn*. 1967;2(1):29–34.
10. Salamon TR, Armstrong RC, Brown RA. Travelling waves on inclined films: numerical analysis by the finite element method. *Phys Fluids*. 1994;6:2202–2220.
11. Gao P, Morley NB, Dhir V. Numerical simulation of wavy falling film flow using VOF method. *J Comput Phys*. 2003;192:624–642.
12. Xu ZF, Khoo BC, Wijeysundera NE. Mass transfer across the falling film: simulations and experiments. *Chem Eng Sci*. 2008;63:2559–2575.
13. Alekseenko SV, Nakoryakov VE, Pokusaev BT. *Wave Flow of Liquid Films*. New York: Begel House, Inc., 1994;313.
14. Chang HC, Demekhin EA. *Complex Wave Dynamics on Thin Films*. Amsterdam: Elsevier. 2002;412.
15. Shkadov VYa, Sisoev GM. Waves induced by instability in falling films of finite thickness. *Fluid Dyn Res*. 2004;35(5):357–389.
16. Shkadov VYa, Sisoev GM. Numerical bifurcation analysis of the travelling waves for a falling liquid film. *Comput Fluids*. 2005;34(2):151–168.
17. Sisoev GM. Bifurcation of attractor in falling film problem. *Int J Non-Linear Mech*. 2008;43:246–263.
18. Yih CS. Stability of liquid flow down an inclined plane. *Phys Fluids*. 1963;6(3):321–334.
19. Kao TW. Stability of two-layer viscous stratified flow down an inclined plane. *Phys Fluids*. 1965;8:812.
20. Kao TW. Role of the interface in the stability of stratified flow down an inclined plane. *Phys Fluids*. 1965;8:2190.
21. Kao TW. Role of viscosity stratification in the stability of two-layer flow down an incline. *J Fluid Mech*. 1968;33:561.
22. Sisoev GM, Shkadov VYa. Instability of two-layer film flow along an inclined surface. *Fluid Dyn*. 1992;27(2):160–165.
23. Chen KP. Wave formation in the gravity-driven low-Reynolds number flow of two liquid films down an inclined plane. *Phys Fluids A*. 1993;5(12):3038–3048.
24. Hu J, Millet S, Botton V, Hadid HB, Henry D. Inertialess temporal and spatio-temporal stability analysis of the two-layer film flow with density stratification. *Phys Fluids*. 2006;18:104101.
25. Hu J, Yin XY, Hadid HB, Henry D. Linear temporal and spatiotemporal stability analysis of the two-layer falling film flows with density stratification. *Phys Rev E*. 2008;77:026302.
26. Çekiç G, Sisoev GM. Dominating wave regimes in a two-layer film flowing down a vertical plane. *Phys Fluids*. 2014;26:122111.
27. Çekiç G, Sisoev GM. On wave families in a two-layer falling film. *Int J Non-Linear Mech*. 2015;69:45–54.
28. Emmert RE, Pigford RL. A study of gas absorption in falling liquid films. *Chem Eng Prog*. 1954;50(2):87–93.
29. Jepsen JC, Crosser OK, Perry RH. The effect of wave induced turbulence on the rate of absorption of gases in falling liquid films. *AIChE J*. 1966;12(1):186–192.
30. Muenz K, Marchello JM. Surface motion and gas absorption. *AIChE J*. 1966;12(2):249–253.
31. Oliver DR, Atherinos TE. Mass transfer to liquid films on an inclined plane. *Chem Eng Sci*. 1968;23:525–536.
32. Goren SL, Mani RVS. Mass transfer through horizontal liquid films in wavy motion. *AIChE J*. 1968;14(1):57–61.
33. Henstock WH, Hanratty TJ. Gas absoption by a liquid layer flowing on the wall of a pipe. *AIChE J*. 1979;25(1):122–131.
34. Yoshimura PN, Nosoko T, Nagata T. Enhancement of mass transfer into a falling laminar liquid film by two-dimensional surface waves - some experimental observations and modeling. *Chem Eng Sci*. 1996;51(8):1231–1240.
35. Wasden FK, Dukler AE. A numerical study of mass transfer in free falling wavy films. *AIChE J*. 1990;36(9):1379–1390.

Manuscript received Nov. 4, 2014, and revision received Feb. 1, 2015.